GEOPHYSICAL RESEARCH LETTERS, VOL. 36, L03104, doi:10.1029/2008GL036535, 2009

Full-wave modeling of transionospheric propagation of VLF waves

Nikolai G. Lehtinen[1] and Umran S. Inan[1]

Received 30 October 2008; revised 16 December 2008; accepted 2 January 2009; published 12 February 2009.

[1] The full-wave method (FWM) of N. G. Lehtinen and U. S. Inan (2008) is used to model trans-ionospheric propagation of VLF electromagnetic waves from ground-based transmitters up to satellite altitudes. Direct comparison with satellite observations indicates that the VLF wave intensities measured at satellite altitudes are substantially smaller than predicted. The apparent reduction in amplitude is attributed to the presence of irregularities in the ionosphere, which the waves encounter during their traversal of the lower ionosphere. Linear mode scattering from the irregularities convert the whistler waves into quasi-electrostatic whistler mode (QEWM) waves with wave normal angles near the resonance cone. Recent enhancements to the FWM are also described, which allow the minimization of an aliasing error encountered in taking the inverse Fourier transform. **Citation:** Lehtinen, N. G., and U. S. Inan (2009), Full-wave modeling of transionospheric propagation of VLF waves, *Geophys. Res. Lett.*, *36*, L03104, doi:10.1029/2008GL036535.

1. Introduction

[2] The very low frequency (VLF, <30 kHz) powerful ground-based transmitters excite waves that propagate in the Earth-ionosphere waveguide, with some radiation continually leaking upward through the ionosphere and up to the magnetosphere, where it can be detected by satellites. Recently *Starks et al.* [2008] compared data from five satellites with calculations using several models of trans-ionospheric VLF propagation combined with a three-dimensional ray tracing in ionosphere. The trans-ionospheric propagation modeling included absorption in the lower ionosphere and reflection from the lower ionospheric boundary. It was found that the calculations overestimate the VLF field in non-equatorial regions by 23 dB at night and by 10 dB during the day. Proposed explanations included enhanced *D* region reflectivity due to transmitter modification, scattering from transmitter-induced irregularities, and conversion to non-propagating lower hybrid modes. The presence of ionospheric irregularities was consistently observed by *Parrot et al.* [2007] above NWC transmitter. These perturbations are likely caused by the powerful VLF radiation from NWC, and include strong plasma wave turbulence, fluctuations of electron and ion densities, and increased temperature. In this paper, we utilize a new enhanced version of a recently developed full-wave model of trans-ionospheric propagation of ELF/VLF waves to quantitatively determine the electric and magnetic field intensities of signals from two different ground-based sources and directly compare results with satellite observations.

2. Full-Wave Method Enhancements

2.1. Method Overview

[3] The full-wave method (FWM) [*Lehtinen and Inan*, 2008] is a method by which the electromagnetic field created by an arbitrary configuration of sources at fixed frequency $\sim e^{-i\omega t}$ can be found in an arbitrary non-magnetic ($\mu \equiv 1$) plane-stratified medium which is uniform in the horizontal (x, y)-direction. In the vertical z-direction the changes in the medium are described in terms of layers with fixed dielectric permittivity tensor $\hat{\varepsilon}$ in each layer. By Snell's law, the horizontal wave vector $\mathbf{k}_\perp$ is conserved during propagation through all layers. Based on this fact, the sources of arbitrary spatial shape are first expanded in their horizontal Fourier components $\sim e^{i(\mathbf{k}_\perp \cdot \mathbf{r}_\perp)}$. The electromagnetic field $\mathbf{E}(\mathbf{k}_\perp)$, $\mathbf{H}(\mathbf{k}_\perp)$ is found for each $\mathbf{k}_\perp$ in the following manner. The full-wave field is separated into two upward- and two downward-propagating modes in each layer. The reflection coefficients (which transform upward modes into downward modes and vice versa) and mode amplitudes are calculated recursively in a direction which provides stability against the numerical "swamping", which is inherent in many similar methods [*Budden*, 1985, pp. 574–576]. The fields in adjacent layers are linked by the boundary conditions on $\Delta\mathbf{E}_\perp$ and $\Delta\mathbf{H}_\perp$ at each layer boundary. These conditions are simply $\Delta\mathbf{E}_\perp = 0$, $\Delta\mathbf{H}_\perp = 0$ in the absence of sources, and are proportional to external electric and magnetic currents which flow inside the layer boundaries (we collapse all volume sources onto the boundary surfaces, so that the waves inside each layer are described by source-free modes). Finally, the inverse Fourier transform $\mathbf{k}_\perp \rightarrow \mathbf{r}_\perp$ is applied to find $\mathbf{E}(\mathbf{r}_\perp)$, $\mathbf{H}(\mathbf{r}_\perp)$. Below we discuss the aliasing problem occurring when the continuous Fourier transform is replaced with a discrete transform, and a method to work around this problem.

2.2. Aliasing Problem in the Inverse Fourier Transform

[4] The inverse Fourier transform in the transverse coordinates was initially implemented numerically by *Lehtinen and Inan* [2008] as a discrete transform using a uniformly spaced rectangular grid for $\mathbf{k}_\perp = (k_x, k_y)$ and $\mathbf{r}_\perp = (x, y)$, which allows utilization of the Fast Fourier Transform (FFT) algorithm. However, close examination indicated that for point sources, such as a ground-based dipole transmitter, this approach is not the most efficient because of the presence of resonances in $\mathbf{k}_\perp$. These resonances are due to reflections from the Earth surface and the lower ionospheric boundary, correspond to waveguide modes and have a width of the order of $1/r_{\mathrm{att}}$ where r_{att} is the mode

[1]Space, Telecommunications and Radioscience Laboratory, Electrical Engineering Department, Stanford University, Stanford, California, USA.

0094-8276/09/2008GL036535$05.00

attenuation distance. Even in the absence of such reflections, i.e., in vacuum, the field in $\mathbf{k}_\perp$-space achieves an infinite value at $|\mathbf{k}_\perp| = k_0 = \omega/c$ (i.e., $|\mathbf{n}_\perp| = 1$), which represents a spherical wave propagating away from the source. If one uses an uniformly spaced grid, the result has aliased sources located at distance $L = 2\pi/\Delta k$, where Δk is the grid step in $\mathbf{k}_\perp$ domain. The interference from these aliased sources can be diminished by taking very small Δk. Since the fields decrease relatively slowly as $L^{-1/2}$ in the Earth-ionosphere waveguide, realization of a given relative error of $\epsilon = \sqrt{r/L}$ requires the use of step sizes of $\Delta k = 2\pi\epsilon^2/r$, where r is the distance of interest. Thus, to decrease the error just by a factor of two, Δk has to be decreased by a factor of four, and the amount of calculations is increased by a factor of 16, because $\mathbf{k}_\perp$ has two dimensions. The use of a uniform grid thus becomes inefficient when the interference from the aliased sources is important.

[5] To properly implement the inverse Fourier transform requires integration through the resonances (in the vacuum case, through a singularity). Desired accuracy can be achieved by using more integration points in the vicinity of the resonance. On the other hand, to preserve computational efficiency, a sparser integration grid is used at values of $\mathbf{k}_\perp$ far from the resonances. Since the location of the resonances is not known in advance, an adaptive integration algorithm is used to find the optimal integration grid. To simplify the determination of the optimal grid, advantage is taken of the fact that the resonances take place approximately at circumferences $|\mathbf{k}_\perp| \approx const$. This property is due to the fact that the ionosphere reflection height depends weakly on the geomagnetic field. Thus, a polar coordinate grid is chosen with points located at intersections of circles $|\mathbf{k}_\perp| = const$ and rays $\chi = const$, where χ is the azimuthal angle in the (k_x, k_y) plane. The points $\chi = const$ are chosen to be uniformly distributed, while the points for $|\mathbf{k}_\perp|$ are chosen using the simple adaptive algorithm described below.

[6] By expanding the integrated function $f(x)$ in Taylor series, we obtain an approximate expression for an integral over a small interval d:

$$\int_{-d/2}^{d/2} f(x)\,dx = f(0)d + \frac{d^3}{24}f''(0) + O(d^5) \tag{1}$$

The rectangle (or midpoint) method of numerical integration is represented by keeping only the first term in this expansion. The error is approximately equal to the second term $\varepsilon = (d^3/24)|f''(0)|$. The total error of integration over N intervals is

$$\mathrm{E} = \sum_{i=1}^{N} \varepsilon_i = \sum_{i=1}^{N} \frac{d_i^3}{24}|f''(x_i)| \tag{2}$$

where $d_i = x_{i+1/2} - x_{i-1/2}$ is the length and $x_i = (x_{i+1/2} + x_{i-1/2})/2$ is the central value of i-th interval. The optimal grid is chosen by minimizing N while requiring constraints $d_i \le d_0$ and $\mathrm{E} \le \mathrm{E}_0$, with fixed d_0, E_0 and boundaries $a = x_{1/2}$, $b = x_{N+1/2}$. In practice, we require that all intervals contribute a small fixed error $\varepsilon_i \le \varepsilon_0$ where we use an estimate $\varepsilon_0 = \mathrm{E}/N_0$ with $N_0 = (b - a)/d_0$. It is therefore required that

$$d_i = \min\left\{d_0, \sqrt[3]{\frac{24\varepsilon_0}{|f''(x_i)|}}\right\} \equiv D(x_i) \tag{3}$$

We can construct the grid from function $D(x)$ by introducing

$$U(x) = \int_a^x \frac{dx}{D(x)} \tag{4}$$

so that $U(x_{i+1/2}) - U(x_{i-1/2}) \simeq d_i/D(x_i) = 1$ and we have

$$U(x_{i+1/2}) = \int_a^{x_{i+1/2}} \frac{dx}{D(x)} \simeq i \tag{5}$$

The number of points N is $U(b)$ rounded upward, and the grid is found using the inverse function $X(i) \equiv U^{-1}(i)$:

$$x_{i+1/2} = X(i), \qquad i = 0 \ldots N \tag{6}$$

[7] For the implementation of the inverse Fourier transform, the minimum step d_0 is Δk, which is determined by the distances of interest r, i.e. $\Delta k = 2\pi/r$. In the vicinity of waveguide resonances, the step calculated by above algorithm is $\sim\varepsilon_0^{1/3}/r_{\mathrm{att}}$. Thus, each resonance contributes only $O(\varepsilon_0^{-1/3})$ different values of $|\mathbf{k}_\perp|$. Therefore, the resonances contribute just a small fraction to the total volume of calculation. The number of different values of $\mathbf{k}_\perp$ remains of the order $N = (k_{\max}/\Delta k)^2 \propto r^2$, even in the presence of resonances. If we were to use the old FFT approach, we would have to use $\Delta k_{\mathrm{FFT}} = 2\pi/r_{\mathrm{att}}$, and $N_{\mathrm{FFT}} \propto r_{\mathrm{att}}^2$. This would be inefficient if we want to limit our calculations to distances $r \ll r_{\mathrm{att}}$.

3. Trans-ionospheric VLF Propagation

[8] We now apply the FWM with its new robust inverse Fourier transform implementation to calculate the VLF radiation from a ground-based vertical electric dipole. The major losses in trans-ionospheric transmission are due to absorption in ionosphere resulting from electron-neutral collisions. Above altitudes of ~110–120 km, the collisions are negligible. If a smooth undisturbed ionosphere profile is used above 110 km (such as produced by IRI model [*Bilitza*, 2001]), the whistler waves propagate in this region virtually without attenuation. The use of planar stratified model is justified by small distances of calculation (<500 km), at which the curvature of the Earth or the change of the geomagnetic field is not too significant.

[9] We consider two specific examples: (1) Omega D transmitter situated near La Moure, North Dakota, USA, which was a part of Omega Navigation System until its shutdown on September 30, 1997; and (2) NWC transmitter, also known as Naval Communication Station Harold E. Holt, located near the town of Exmouth, Western Australia.

3.1. Omega D Transmitter

[10] We now compare the results of FWM calculations with satellite observations presented by *Inan et al.* [1984].

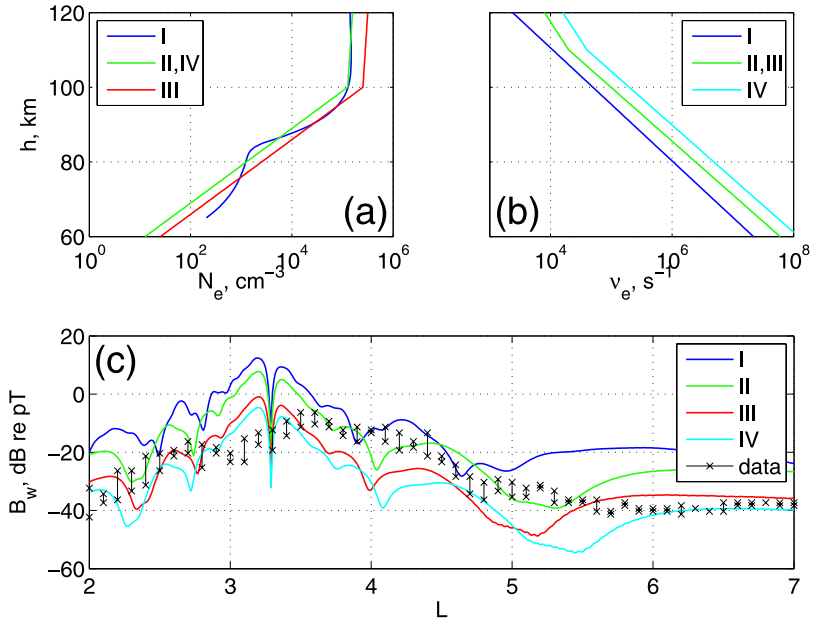

Figure 1. Omega D transmitter case: parameter profiles used in runs I–IV and calculation results: (a) electron density, (b) electron-neutral collision frequency, and (c) the wave magnetic field at DE-1 satellite calculated by FWM, with satellite data from *Inan et al.* [1984] shown with vertical bars.

At that time, Omega D transmitter was operating at frequency $f = 13.1$ kHz, with power of $P = 10$ kW. Observations of the VLF field by DE-1 satellite were made at 4000 km altitude. The maximum observed value of the wave magnetic field was $B_w = -6$ dB re pT. *Inan et al.* [1984] also presents a comparison with theoretical value of the field, which was calculated using previous approximate results of *Helliwell* [1965, Figure 3–35] for transionospheric propagation of plane waves. That calculation used QL approximation for whistlers (and thus ignored the direction of the geomagnetic field), and neglected full-wave effects, such as reflections from the ionosphere boundary. However, the last effect is probably not so important since the VLF waves reflected by the ionosphere are reflected again by the Earth, i.e., the reflection of the waves from the ionospheric boundary does not necessarily contribute to reduction of the field that escapes upward.

[11] To apply the FWM, we first calculate the value of the current moment in the vertical dipole antenna, knowing the radiated power. In vacuum, the current moment Il and radiated power P are related by

$$P = \frac{Z_0 k_0^2 (Il)^2}{12\pi} \tag{7}$$

where $Z_0 = \sqrt{\mu_0/\epsilon_0}$ is the vacuum impedance and $k_0 = \omega/c = 2\pi f/c$. When perfectly conducting Earth is present, we have to take into account the image current and the fact that radiation is only into upper half-space, which specifies the current moment as

$$Il = \sqrt{\frac{6\pi P}{Z_0 k_0^2}} \tag{8}$$

The FWM calculations are performed for several runs, featuring various daytime electron density (N_e) and electron-neutral collision frequency (ν_{en}) profiles, with the following parameters (see Figures 1a and 1b):

$$\text{I. } N_e = N_e^{[\text{IRI}]},\ \nu_{en} = \nu_{en}^{[\text{V02}]}$$
$$\text{II. } N_e = N_e^{[\text{H65}]},\ \nu_{en} = \nu_{en}^{[\text{H651}]}$$
$$\text{III. } N_e = 2N_e^{[\text{H65}]},\ \nu_{en} = \nu_{en}^{[\text{H65}]}$$
$$\text{IV. } N_e = N_e^{[\text{H65}]},\ \nu_{en} = 2\nu_{en}^{[\text{H65}]}$$

where $N_e^{[\text{IRI}]}$ is the electron density profile obtained using IRI model [*Bilitza*, 2001] for daytime conditions similar to those at the time of observation, $\nu_{en}^{[\text{V02}]}$ is a collision frequency profile based on recent observations [*Vuthaluru et al.*, 2002], $N_e^{[\text{H65}]}$ and $\nu_{en}^{[\text{H65}]}$ are daytime electron density and collision profile on which the calculations of *Inan et al.* [1984] were based, namely those presented by *Helliwell* [1965, Figure 3–27].

[12] The FWM is applied between altitudes of 0–120 km. The geomagnetic field is taken to be that corresponding to the location of the transmitter at $L = 3.3$, thus having a zenith angle of $\theta_B = 18.2°$. The electromagnetic VLF field and the Poynting vector are calculated at the altitude of 120 km. To transport the fields to the satellite altitude of 4000 km, we assume ducted propagation and spreading of wave power in accordance with the divergence of geomagnetic field lines, corresponding to a reduction in intensity of ~6.8 dB. The wave magnetic field B_w at the satellite is calculated from the Poynting vector by assuming a whistler refractive index of $n_w = 10$, and the ratio $B_w/E_w = n_w/c$ which corresponds to wave normals not too far from the direction of the geomagnetic field.

[13] The results of these calculations are presented in Figure 1c, for the case with the satellite passing along the

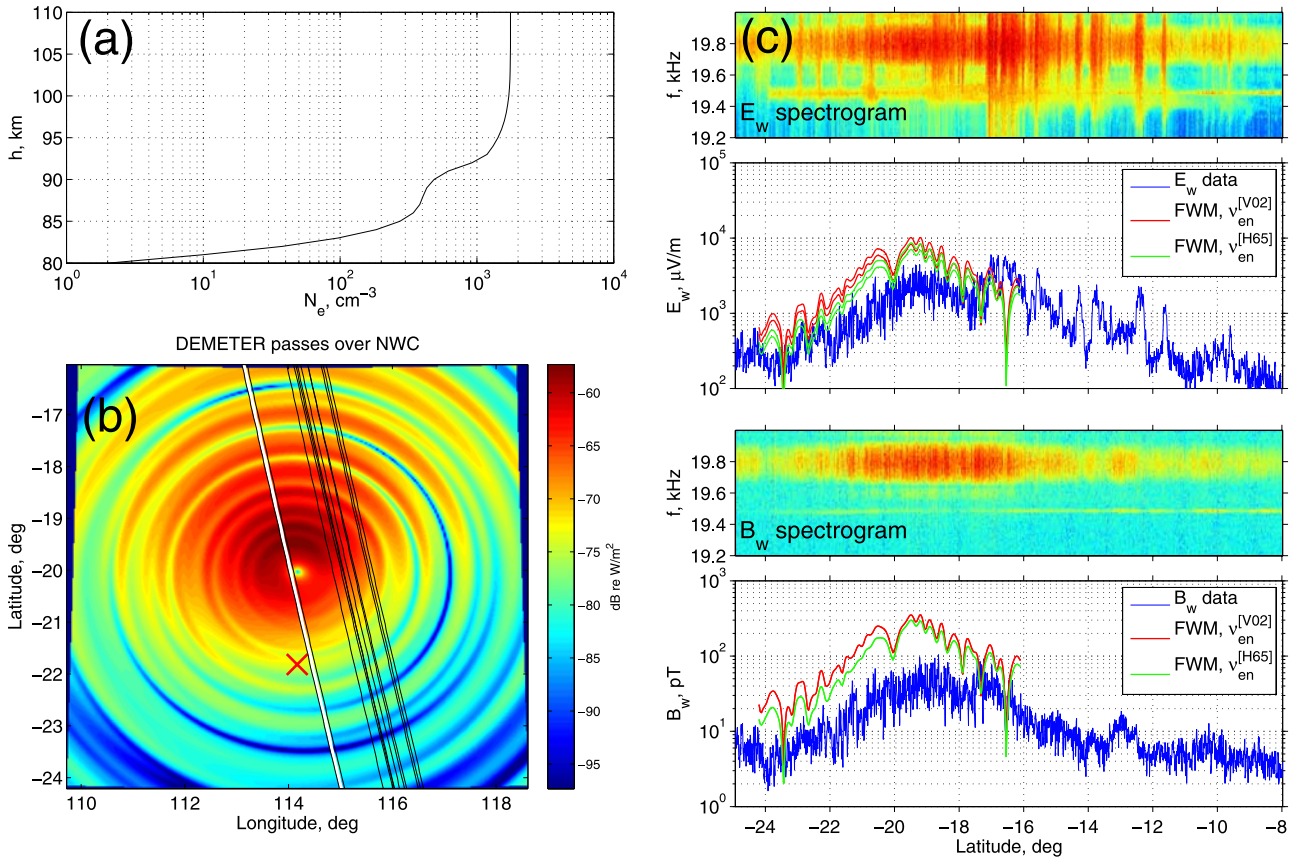

Figure 2. NWC transmitter case: (a) IRI model electron density profile used, (b) the energy flux at the satellite altitude of 700 km, with satellite orbits and location of the source on the ground (cross), and (c) satellite data and results of FWM calculations for pass on October 24, 2006, starting at 14:50:40 UT (white thick line in Figure 2b). The VLF wave fields are calculated for two profiles of ν_e. The line satellite data are filtered around $f = 19.8$ kHz with the bandwidth of $\Delta f \simeq 300$ Hz. The double lines for the FWM calculated fields denote bounds between which the absolute value of elliptically-polarized field oscillates.

geomagnetic meridian exactly above the source. The asymmetry of the field for L-shells lower and higher than the source is due to the fact that the whistler waves penetrate ionosphere easier along the geomagnetic field lines. Upon inspection of the maximum calculated values of B_w for different runs, we conclude that the observed value of $B_w = -6$ dB occurs only for the case of a collision frequency with a very high (unrealistic) value $\nu_{en} = 2\nu_{en}^{[H65]}$. For realistic values of N_e and ν_{en}, the calculated wave field is much larger (by $\sim$10 dB) than that observed and also that which is calculated by *Inan et al.* [1984] using the simple model. The fact that the dominant peaks in the satellite data and in the calculated field are not perfectly aligned might be due to the fact that at lower altitudes ($\lesssim$1000 km) the propagation is non-ducted; the same effect is seen in calculations of *Starks et al.* [2008, Figure 4].

3.2. NWC Transmitter

[14] We now analyze VLF data from DEMETER satellite passing over NWC transmitter. We analyzed 13 passes that occurred in September–November of 2005–2008, at $\sim$22:30 LT. The transmitter has carrier frequency $f = 19.8$ kHz and power $P = 1$ MW. The radiating current moment is again calculated from equation (8). The geomagnetic field $\mathbf{B}_E$ is calculated from IGRF model [*Macmillan et al.*, 2003] and has a rather high deviation from the zenith, $\theta_B = 34.6°$. The FWM is applied to calculate the field and energy flux at an altitude of 110 km, using the electron density profile N_e obtained from IRI model [*Bilitza*, 2001] (Figure 2a). Two cases are considered with different collision frequency profiles $\nu_{en} = \nu_{en}^{[V02]}$ and $\nu_{en} = \nu_{en}^{[H65]}$, described previously.

[15] Non-ducted propagation is assumed to map the field from 110 km to the DEMETER orbit altitude of 700 km, with the group velocity $\mathbf{v}_g$ direction of the VLF wave packet being between $\mathbf{B}_E$ and the vertical (in collisionless plasma). The energy flux at the satellite altitude is presented in a 2D plot (Figure 2b), together with the location of the source and the analyzed passes. The concentric circles are caused by interference of VLF waveguide modes in the Earth-ionosphere waveguide. The center of these circles maps to the location of the VLF transmitter on the ground, the latitudinal displacement being due to the direction of the group velocity of the VLF waves. As in the case of Omega D transmitter, the asymmetry of the circles is due to the fact that the whistler waves penetrate through the ionosphere easier along the $\mathbf{B}_E$ lines.

[16] The calculated electric (E_w) and magnetic (B_w) field at the satellite orbit are plotted, together with the observations, in Figure 2c for the pass that occurred on October 24,

2006, starting at 14:50:40 UT. We see that both E_w and B_w are greater than the observed fields at their maximum (latitudes $\simeq -19.5°$). Outside the maximum (at latitudes $\gtrsim -17°$), the observed E_w at times actually exceeds the calculated values, displaying bursts of a relatively small-scale (compared to the distance to the source) structure. The Doppler-shift broadening of the signal due to the motion of the satellite is shown in the spectrograms, and is greater at the location of these bursts. Other 12 analyzed passes exhibit similar features. On the basis of a visual inspection of field plots we found that small-scale structures are present in 12 out of 13 passes. From these, in 3 passes the structures are present in both E_w and B_w, and in 9 passes only in E_w. All 13 passes exhibit smaller than calculated field around the maximum, by an average of $\simeq$8 dB for E_w and by $\simeq$14 dB for B_w. The smaller attenuation of E_w may be interpreted as the E_w-field structures being superimposed over the maximum.

4. Summary and Discussion

[17] The new full-wave method (FWM) is applied to calculate the electromagnetic field in the stratified ionosphere for ground-based dipole transmitters and compared to observations in two different cases, Omega D and NWC transmitter. The mapping to satellite altitude is done using ducted (for high-altitude orbit of DE-1 in the first case) or non-ducted (for low-altitude orbit of DEMETER in the second case) propagation. In both cases, we found that the observed field values are relatively low compared to calculation results, in regions close to the maximum field amplitudes, in agreement with analysis of *Starks et al.* [2008]. The attenuation of the waves in their transionospheric propagation to the satellite altitudes in both cases is evidently more than that due to simple collisional absorption in the lower ionosphere. Moreover, for the NWC case (Figure 2c), in regions far from the maximum (at latitudes $\gtrsim -17°$), the observed E_w actually exceeds the calculated values, and also shows relatively small-scale (compared to the distance from the source) structures, which exhibit a significant Doppler broadening.

[18] We have ruled out an increased collisional absorption as the cause of the larger than expected attenuation of VLF waves by varying input parameters N_e and ν_{en} (see Omega D transmitter case). Therefore, we attribute additional attenuation and appearance of small-scale structures to scattering of VLF waves from structures of a relatively small scale, such as field-aligned irregularities. This leads to substantial conversion of the energy of 0^+ whistler-mode waves into quasi-electrostatic whistler mode (QEWM) waves [*Bell and Ngo*, 1990; *Bell et al.*, 2008], which manifests itself in wave energy deficit (compared to calculations) in some regions and excess in others. The irregularities are likely caused by the powerful emission from NWC transmitter, as their presence was consistently observed by *Parrot et al.* [2007]. The signal from Omega D had traveled a greater distance to the satellite and therefore could experience additional scattering at higher altitudes.

[19] The waves calculated by FWM are 0^+ whistler-mode waves that propagate in a strictly horizontally stratified medium, and therefore have small $\mathbf{k}_\perp$ (i.e., $|\mathbf{k}_\perp| \lesssim k_0 = \omega/c$ due to Snell's law conservation of $\mathbf{k}_\perp$). The direction of their group velocity $\mathbf{v}_g$ is between $\mathbf{B}_0$ and the vertical, and they have a substantial magnetic field component $cB_w \simeq n_w E_w$, with whistler refractive index $n_w \simeq 12$ at DEMETER altitude. In contrast, QEWM waves have high values of $\mathbf{k}_\perp$, i.e. their wave normals lie very near the resonance cone. The direction of $\mathbf{v}_g$ is close to $\mathbf{B}_0$, and the field has quasi-electrostatic properties $E_w \gg cB_w$ and $\mathbf{E}_w \parallel \mathbf{k}$.

[20] We propose that the structures in Figure 2c at latitudes $\gtrsim -17°$ are due to QEWM waves. The location of the structures is explained by the difference in the group velocity direction, the QEWM waves being deflected away from the vertical propagation more than 0^+ whistler modes. The quasi-electrostatic nature is consistent with the absence of structure in the magnetic field records. The significant Doppler shifts inside the structures (shown in spectrograms of Figure 2c) are also a strong supporting argument for the presence of QEWM waves, which have large $|\mathbf{k}_\perp|$.

[21] **Acknowledgments.** This work was supported by the High-Frequency Active Auroral Research Program (HAARP), the Air Force Research Laboratory (AFRL), the Defense Advanced Research Program Agency (DARPA), and the Office of Naval Research (ONR) via ONR grant N00014-05-1-0854 to Stanford University. We are grateful to Michel Parrot at LPCE/CNRS (France) for the DEMETER satellite data and to Kevin Graf for extracting the data for the DEMETER NWC passes.

References

Bell, T. F., and H. D. Ngo (1990), Electrostatic lower hybrid waves excited by electromagnetic whistler mode waves scattering from planar magnetic-field-aligned plasma density irregularities, *J. Geophys. Res.*, *95*, 149–172.

Bell, T. F., U. S. Inan, D. Piddyachiy, P. Kulkarni, and M. Parrot (2008), Effects of plasma density irregularities on the pitch angle scattering of radiation belt electrons by signals from ground based VLF transmitters, *Geophys. Res. Lett.*, *35*, L19103, doi:10.1029/2008GL034834.

Bilitza, D. (2001), International reference ionosphere 2000, *Radio Sci.*, *36*, 261–271, doi:10.1029/2000RS002432.

Budden, K. G. (1985), *The Propagation of Radio Waves: The Theory of Radio Waves of Low Power in the Ionosphere and Magnetosphere*, Cambridge Univ. Press, Cambridge, U. K.

Helliwell, R. A. (1965), *Whistlers and Related Ionospheric Phenomena*, Stanford Univ. Press, Stanford, Calif.

Inan, U. S., H. C. Chang, and R. A. Helliwell (1984), Electron precipitation zones around major ground-based VLF signal sources, *J. Geophys. Res.*, *89*, 2891–2906.

Lehtinen, N. G., and U. S. Inan (2008), Radiation of ELF/VLF waves by harmonically varying currents into a stratified ionosphere with application to radiation by a modulated electrojet, *J. Geophys. Res.*, *113*, A06301, doi:10.1029/2007JA012911.

Macmillan, S., et al. (2003), The 9th-generation international geomagnetic reference field, *Geophys. J. Int.*, *155*, 1051–1056, doi:10.1111/j.1365-246X.2003.02102.x.

Parrot, M., J. A. Sauvaud, J. J. Berthelier, and J. P. Lebreton (2007), First in-situ observations of strong ionospheric perturbations generated by a powerful VLF ground-based transmitter, *Geophys. Res. Lett.*, *34*, L11111, doi:10.1029/2007GL029368.

Starks, M. J., R. A. Quinn, G. P. Ginet, J. M. Albert, G. S. Sales, B. W. Reinisch, and P. Song (2008), Illumination of the plasmasphere by terrestrial very low frequency transmitters: Model validation, *J. Geophys. Res.*, *113*, A09320, doi:10.1029/2008JA013112.

Vuthaluru, R., R. A. Vincent, D. A. Holdsworth, and I. M. Reid (2002), Collision frequencies in the D-region, *J. Atmos. Sol. Terr. Phys.*, *64*, 2043–2054, doi:10.1016/S1364-6826(02)00220-1.

U. S. Inan and N. G. Lehtinen, STAR Laboratory, Stanford University, 350 Serra Mall, Stanford, CA 94305, USA. (nleht@stanford.edu)